Hindawi
Adsorption Science & Technology
Volume 2022, Article ID 3631584, 14 pages
https://doi.org/10.1155/2022/3631584

Research Article

Adsorption and Photocatalytic Degradation Properties of Bimetallic Ag/MgO/Biochar Nanocomposites

R. Venkatesh,[1] **P. Raja Sekaran**,[2] **K. Udayakumar**,[2] **D. Jagadeesh**,[3] **K. Raju**,[4] **and Melkamu Beyene Bayu**[5]

[1]*Department of Mechanical Engineering, Saveetha School of Engineering, SIMATS, Chennai, 602105 Tamil Nadu, India*
[2]*Department of Mechanical Engineering, Er. Perumal Manimekalai College of Engineering, Hosur, 635117 Tamil Nadu, India*
[3]*Department of Mechanical Engineering, Kongunadu College of Engineering and Technology, Trichy, 621215 Tamil Nadu, India*
[4]*Department of Mechanical Engineering, M. Kumarasamy College of Engineering, 639113 Tamil Nadu, India*
[5]*Department of Mechanical Engineering, Ambo Institute of Technology-19, Ambo University, Ambo, Ethiopia*

Correspondence should be addressed to R. Venkatesh; venkateshr.sse@saveetha.com
and Melkamu Beyene Bayu; melkamu.beyene@ambou.edu.et

Received 25 August 2022; Revised 21 September 2022; Accepted 24 September 2022; Published 13 October 2022

Academic Editor: Debabrata Barik

The Ag/MgO/biochar nanostructures were fabricated using a solvent-free ball milling process as an effective adsorbent. Development of functional materials capable of completely removing organic pollutants from water and their adequate adsorption present challenges. The addition of MgO nanoparticles diffused equally on biochar surfaces in the biochar matrix, according to various characterization data. In decomposing biochar and compressing MgO, powdered metal enhanced mesopores and macropores of nanocomposites. XPS analysis indicates the potential synthesis of modified biochar nanocomposites. Adequate amounts of MgO added to biochar improved the ability of the nanocomposites to remove methylene blue (M.B.) through photosynthesis and adsorption. Photocatalytic analysis was carried out for the proposed novel composites to remove tetracycline (T.C.) subjected to different conditions. The photodegradation efficiency was found 80.26% for TC concentration, 50 ppm, H_2O_2 of 100 mM pH: 5-6 of Ag/MgO/biochar (0.01 g) at 25° temperature. Treatment of various organic wastewaters by metal oxide/biochar nanocomposites with strong adsorption and photocatalytic degradation capabilities is made possible by this research.

1. Introduction

Wastewater reclamation is required for various applications as a financially efficient and effective technologies for removing harmful contaminants [1, 2]. This approach is preferred in most countries based of water scarcity caused by fluctuating rainfall and inconsistent accessibility to other water sources, especially for cultivation [3, 4]. In terms of wastewater management, this strategy is a better option in light of the emergence of renewable initiatives.

The combined efficiency of adsorption and photocatalytic techniques dramatically increases the applications of biochar/meal oxide nanocomposites [5]. Pretreatment of the substrate with dissolved salts such as $MgCl_2$, $CaCl_2$, $FeCl_3$, and $ZnCl_2$ before pyrolysis is a common approach for producing metal oxide-enhanced biochar [6]. In addition, metal oxides can be significantly reduced or precipitated on pure biochar surfaces. The main difference between the two fabrication techniques is whether or not the metal component is loaded before pyrolysis. Also, all species provide chemical solutions, which are dangerous to the ecosystem. In addition, asymmetric amounts of the two synthesized metal salts may lead to the accumulation of irregular dispersion of metal oxide nanoparticles on top of the biochar [7]. Consequently, developing simple and environmentally safe metal oxide/biochar nanocomposite formulations is necessary.

Ball milling is a solvent-free fabrication technique for synthesis of adsorbent nanocomposite materials due to easy process, environmentally accessibility, low cost, and high quality of materials [8]. Using ball milling techniques increases the

biochar particles' size and improves the biochar's absorbent properties by forming functional groups of the biochar [9]. To obtain the homogeneous distribution of metal oxide nanoparticles and propose the lattice defects for developing the photocatalytic execution [10], the results of this research suggest that ball milling is a quick and easy way to create a nanocomposite of metal oxide and biochar for enhanced high absorption and photocatalytic capabilities.

Over the past two decades, tetracycline (T.C.) has played a significant role due to its inhibitory antibacterial activity against the spread of coronavirus [11]. Tetracyclines (T.C.) are produced by modifying natural tetracycline to form many compounds that are widely antibacterial for humans and wildlife [12]. However, only a tiny portion of those tetracyclines is absorbed by human and animal organs, endangering both humans and the environment. Hence, a proper and effective treatment plan is essential [13].

Several experimental studies performed the determination and evaluation of materials for simultaneous absorption and photolysis of methylene blue (M.B.) from groundwater. This investigation used solvent-free ball milling fabrication techniques to fabricate Ag/MgO/biochar composites. The work has been followed to (i) conduct the XPS analysis for identifying the relation between biochar and their composites which was involved in ball milling techniques, (ii) investigate the performance of adsorption for removal of methylene blue, and (iii) analyze photocatalytic degradation of Ag/MgO/biochar for removal of tetracycline (T.C.) with different pH levels.

2. Materials and Methods

2.1. Preparation of Biochar. The synthesis of Ag/MgO/biochar nanocomposites was prepared with the addition of silver nitrate ($AgNO_3$) -99.9% and magnesium chloride hexahydrate ($MgCl_2.6H_2O$) and methylene blue (M.B.). Chemicals are used correctly and are of diagnostic quality. Distilled water is used to produce organic matter.

2.2. Synthesis of Biochar Nanocomposites. The modified Ag/MgO/biochar was synthesized using the high-energy ball milling method, as shown in Figure 1. At an Mg : Ag weight ratio of 1 : 1 and 2 : 1 wt% ratio of Ag : B.C. and Mg : B.C., 5 g of rice straw flour was mixed with 0.17 g of magnesium chloride hexahydrate ($MgCl_2.6H_2O$) and 0.08 and silver nitrate [14]. A planetary ball mill machine was used to grind 1.8 g of Pb and MgO mixtures at various volume ratios using 600 mL vials filled with 170 g agate balls of 6 mm diameter. The ball mill experiment is operated at 400 rpm for 12 hours with a 1-hour rotation change in direction.

2.3. Adsorption Performance of Ag/MgO/Biochar Nanocomposites. The Ag/MgO/biochar nanocomposites of M.B. removal rate were identified with 30 mg of all combinations of specimen added to 200 mL of 200 mL M.B. solution. They were moved to the surface mixture and stirred for 24 h until equilibrium (25 2°C) was reached. M.B. adsorption on the sample gradually increased during the first 20 min due to the availability of multiple adsorption sites on the adsorbent material [15]. The kinetic adsorption process is enhanced by the functions of mesopores and macropores in Ag/MgO/biochar nanocomposites. The combinations were then passed through 0.22 μm nylon film filters, and the M.B. concentration of the extracted extract was determined using spectrophotometry with a wavelength of 665 nm. Mass balance analysis was used to estimate the amount of M.B. absorbed in the prepared MgO/biochar composites [16]. The adsorption process obtained measurements were simulated using adsorption kinetics and equilibrium adsorption models, and analytical expressions of the modelling techniques are presented in the Supplementary data.

2.4. Photocatalytic Analysis. All samples dispersed in 100 mL of aqueous solution (160 mg/L) using a quartz beaker were subjected to photocatalytic analysis. Consequently, the stirring and irradiation were suspended suddenly under the 250 W LED lamp conditions. The measurement was taken at a particular time interval during the light irradiation for 2 mL of suspension [17]. The methylene blue (M.B.) removal rate was simulated and measured for 1st order and modified Elovich models during the light irradiation. The statistical value of all adsorbent and photocatalyst studies is used [18].

3. Results and Discussion

3.1. XPS Analysis of Ag/MgO/Biochar. XPS analysis of robust surface techniques has been used to determine the ionic properties and interfacial bonding between biochar and their mixtures. Chemical compositions of Ag/MgO/biochar nanocomposites were compatible with the EDS spectrum. According to the results of the XPS examination, N1s, O1s, and C1s are encountered in this study with Ag/MgO/biochar nanocomposites as significant components, as shown in Figure 2. According to Figure 2, the highest peak intensities of C1s are 292.24 eV, 284.65 eV, and 282.45 eV, respectively, and are attributed to C=C, C–C, and C–O bonds. In addition, the C-O peak intensity from 289.57 eV to 292.24 eV changed significantly in the C1s of Ag/MgO@BC nanocomposites, and the C=C diffraction peak was observed from 294.02 eV to 288.24 eV [19]. Both of these changes indicate the conversion of Ag+ into AgNPs and the formation of MgONPs on the exterior of the customized biochar nanocomposites.

The biochar of O1s reaches different peak intensities depending on the binding energy at 535.21 eV, 538.16 eV, and 542.32 eV, respectively, attributed to metallic oxides by lattice oxygen subjected to surface oxygen-assessed functional group [20]. Similarly, O1s of Ag/MgO/biochar spectrum demonstrate that Mg-O bonding with change in intensity of peak at 539.21 eV, 540.26 eV, and 542.36 eV is partly related to change in the concentration of oxygen vacancy. In addition, the N1s spectra of biochar confirmed the existence of C-N at 399 and 403.25 eV, which is expanded to 401.45 and 405.26 eV in Ag/MgO@BC, indicating the synthesis of MgO and their potential interactions

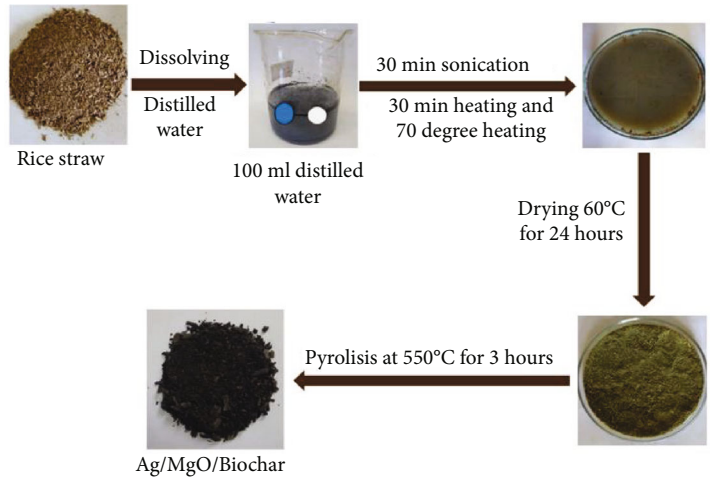

Figure 1: Synthesis of Ag/MgO/biochar.

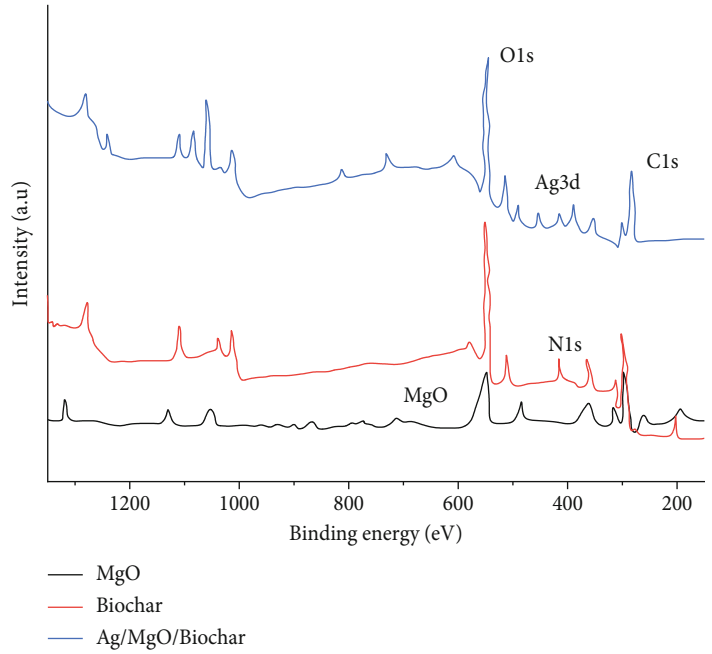

Figure 2: Ag/MgO/biochar XPS spectra.

with AgNPs and N interactions, as shown in Figures 3(a)–3(d).

Ball milling may cause chemical reactions among MgO and biochar in the composites, and the O1s spectra are supported by a slight change in the biochar and their composites (Figures 4(a) and 4(b)). Ball milling involves material interfaces sliding against each other in a friction-like manner, which converts a significant amount of mechanical energy into heat to produce larger parts on regional and macroscopic scales [21]. The extreme temperatures of available regions can cause localized changes and interactions of atoms to form nanocomposites.

Table 1 shows the quantitative analysis of the surface area that established the porous structure of MgO-biochar. During ball milling, the biochar surface area Brunauer-Emmett Teller (BET) improved from 225.7 m^2/g to 280.65 m^2/g, demonstrating that this technique can improve the surface area of biochar. The BET area of MgO is 4.3 m^2/g after the ball milling process when compared to without modified biochar. The specific surface area of Ag/MgO/biochar is 160.2 m^2/g, equal to the definite standardized area. It suggests that high-intensity ball milling using MgO nanoparticles influenced the morphology and interfacial properties of the biochar matrix. In addition, a portion of the nanoparticles dissolved and incorporated into the bioreactor's permeate, reducing the nanocomposites' total active area. Both enlarged surface porous structures and cracks were observed as the biochar, and their blends were broken

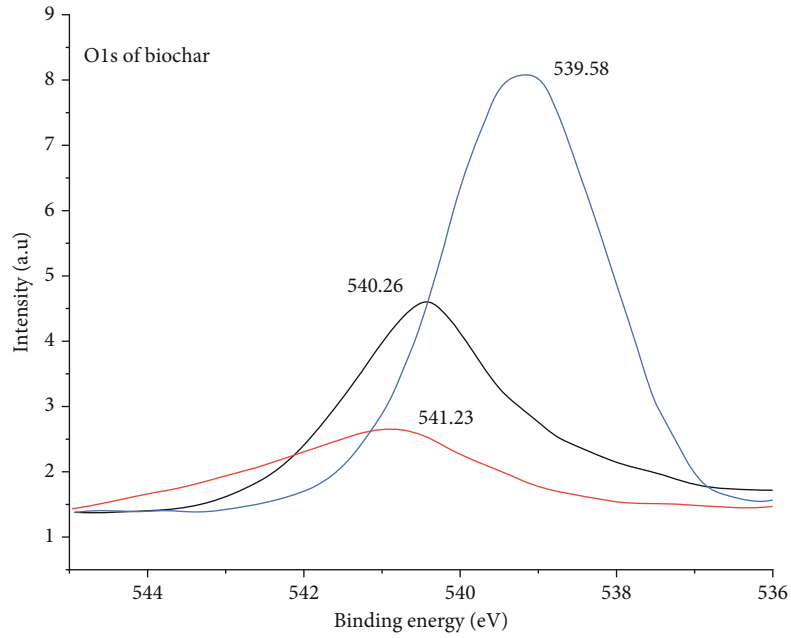

(a)

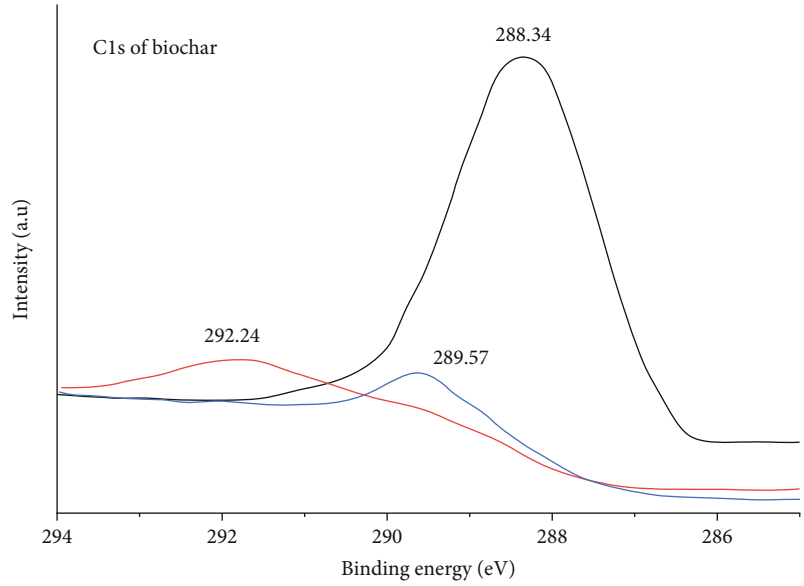

(b)

Figure 3: Continued.

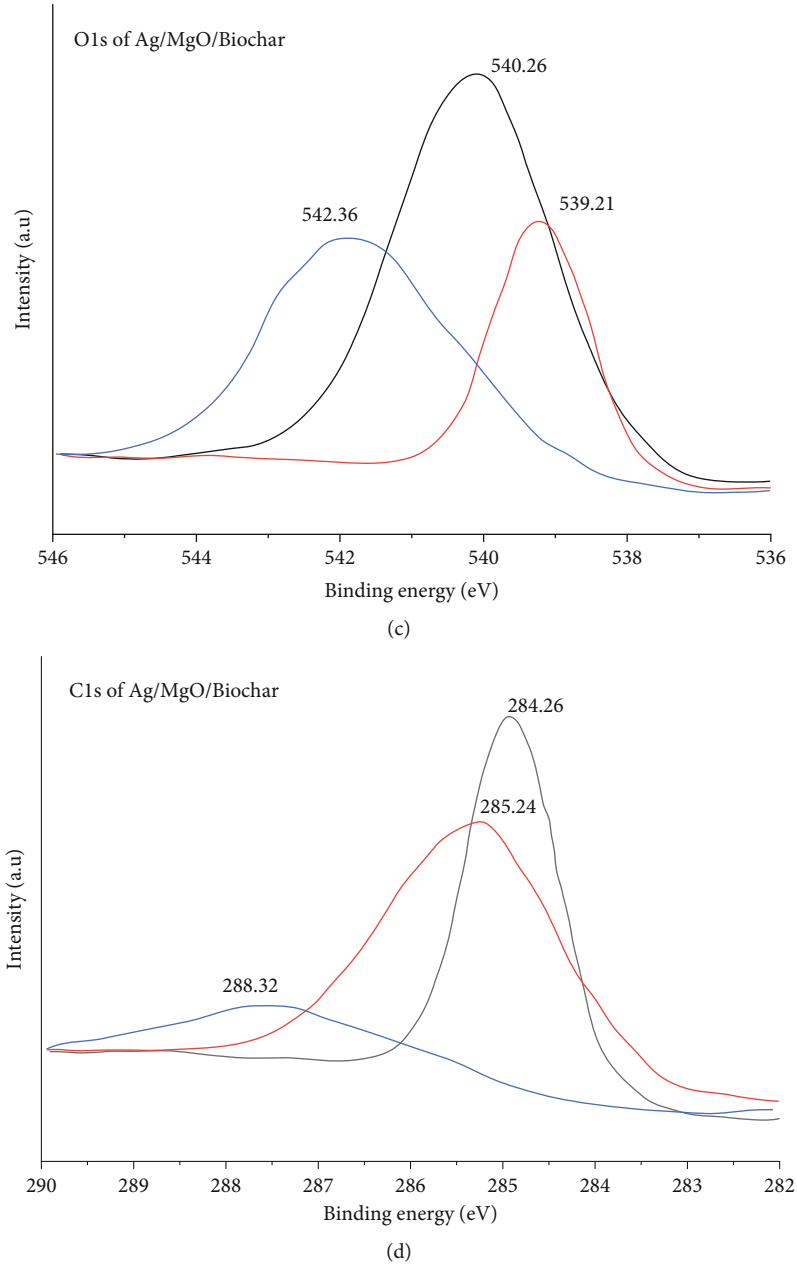

Figure 3: XPS analysis of biochar: (a) O1s biochar; (b) C1s of biochar; (c) O1s of Ag/MgO/biochar; (d) C1s of Ag/MgO/biochar.

into small-sized pieces during the ball milling process [22]. In the nanometre size range, MgO has a great propensity to extrude into the pores and fractures of biochar thermally. Mg_2p spectra of sample Ag/MgO/biochar are shown in Figure 5, with a characteristic peak at 51.46 eV for MgO. This Mg_2p spectrum showed a significant increase compared to BMmix, suggesting that the ball milling method may have had a more profound effect on the composition of the composites than easy mixing [23].

The sample N2 absorption spectra are all according to the classification of type I isotherms, confirming a large number of micropores, as shown in Figure 4. The N2 Adsorption Isotherm Decomposition compared to modified biochar shows apparent abrupt absorption at a relative pressure of 1.0, demonstrating the formation of a significant number of macropores. The distribution of pore sizes in Table 1 shows the presence of numerous micropores, macropores, and micromesopores. MgO/Ag/biochar had a higher specific surface area and maximum pore size than other prepared samples. After the ball milling process significantly increases the macropores and mesopores ($V_{mes} + V_{mac}$), the squeeze of zinc oxide nanoparticles in biochar creates additional porosity and fractures and significantly expands the biochar, whereas grinding can break the biochar into smaller particles and increase the surface area.

3.2. Adsorption Mechanism of M.B. The adsorption process enhances adsorption kinetics due to the accessibility of

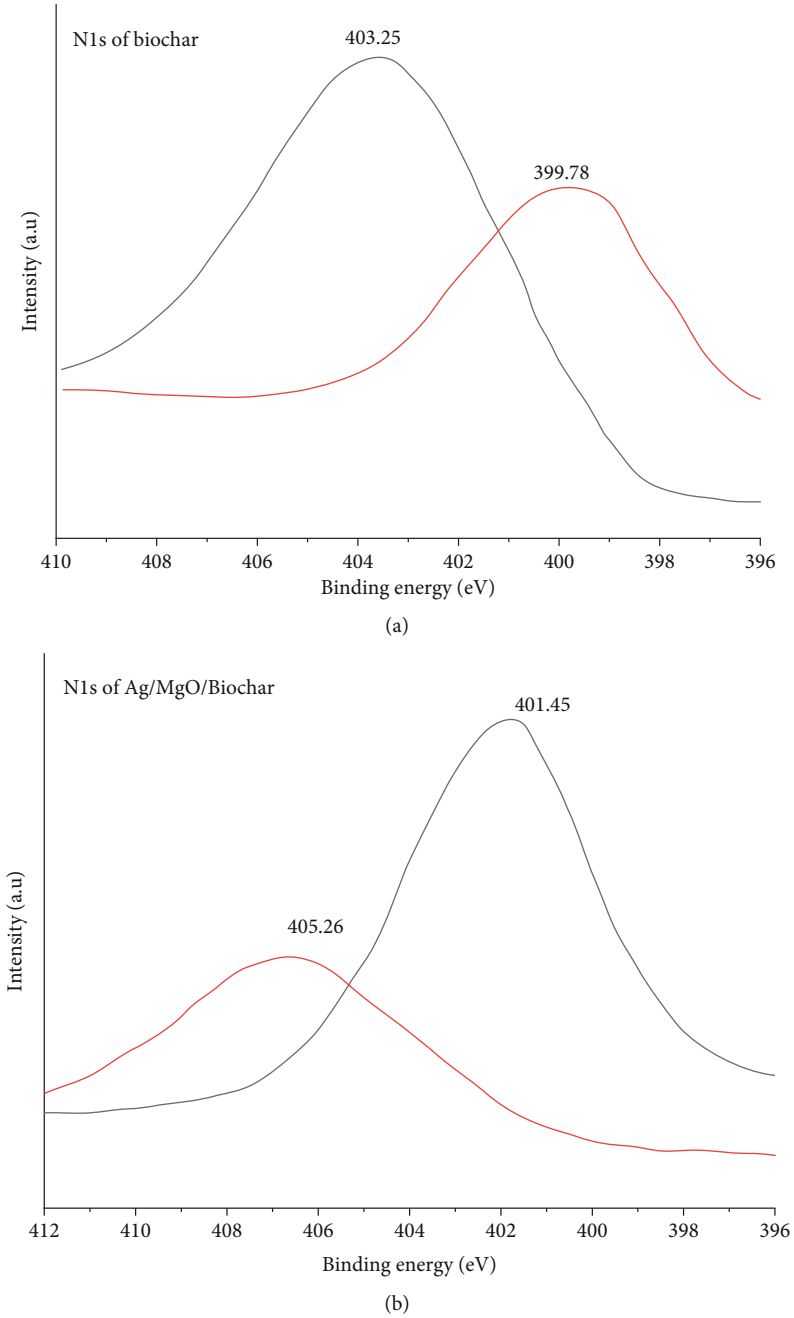

Figure 4: (a) N1s of biochar; (b) N1s of Ag/MgO/biochar.

Table 1: Ag/MgO/biochar physicochemical properties.

Materials	Average size of MgO (nm)	BTE (m^2/g)	BJH pore volume (cm^3/g)
MgO	102	10.52	—
Ag/MgO/biochar	25.6	160.2	0.95
H.C.	—	225.7	0.105
BMHC	—	280.65	0.132

mesopores and macropores. The absorption rate decreased until the absorption mechanism reached 256 min, as shown in Figure 6. The MB pseudosecond-order dynamic model of the adsorption process of nanocomposite membranes is better than the pseudofirst-order model coupled with a coefficient of determination, and also, Langmuir and Freundlich's best fit model is shown in Figure 7. It suggests that multiple processes may have been operating to regulate the adsorption of M.B. on MgO/biochar nanocomposites. The combinations of all nanocomposites had the highest M.B. adsorption, indicating that high MgO loading on biochar would reduce the adsorption capacity of Ag/MgO/biochar

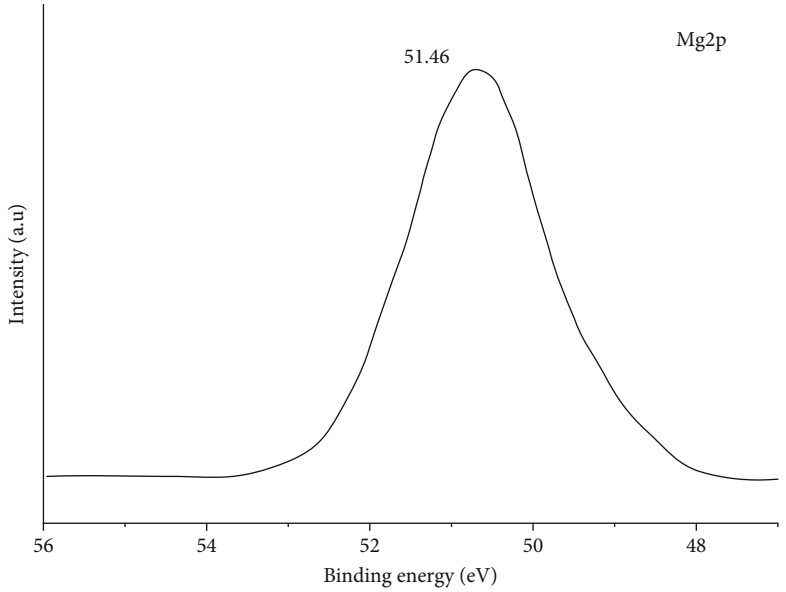

Figure 5: XPS spectra of Mg2p.

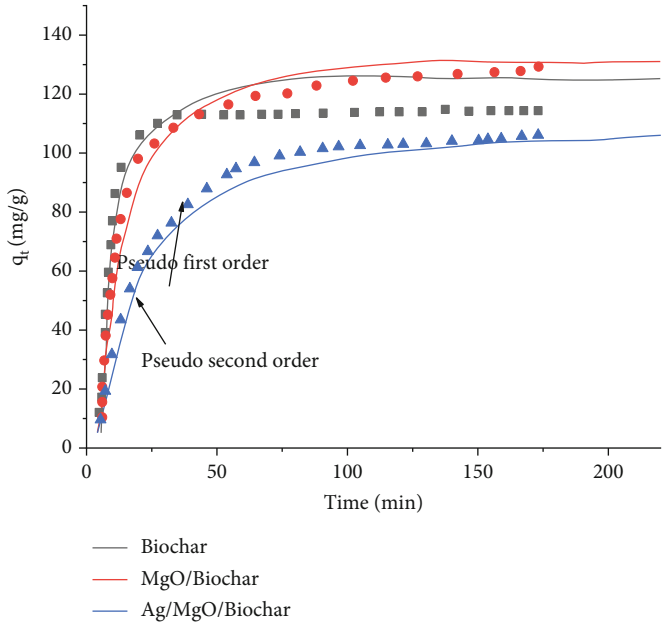

Figure 6: Adsorption kinetics.

composites. As shown in Table 2, adsorption kinetics of R^2 values of 0.991 and 0.925 were obtained for Ag/MgO/biochar for both first- and second-order mock samples, respectively. Table 3 shows the M.B. adsorption for Langmuir and Freundlich's best fit model.

3.3. Adsorption Isothermal of M.B. Recent research has demonstrated that M.B. adsorption in biochar-based nanocomposites can significantly affect electrostatic interactions (Zheng et al., [11]). Freundlich and Langmuir regression analysis was used to calculating the optimal efficiency of M.B. adsorption isothermal. Although the different models, with R^2 values above 0.990, accurately characterized the isothermal models, they could not provide any light on the processes underlying M.B. adsorption on MgO/biochar nanocomposites, as shown in Table 4. All ball-milled samples in this investigation, whether they were MgO or not, had significantly more vital M.B. adsorption capacity than pure B.B. It is considered that adding nanoparticles to biochar throughout ball milling can expand the maximum adsorption areas and promote the electrostatic affinity of M.B. by improving the base equilibrium capacity of

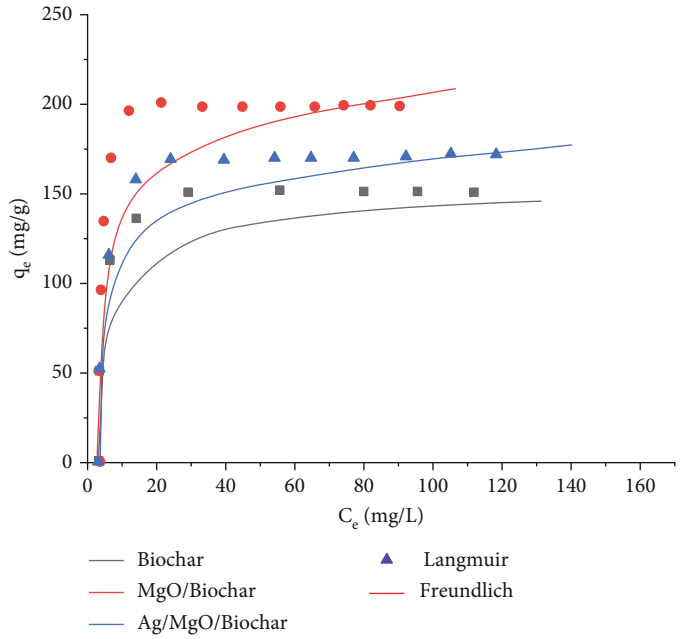

Figure 7: Adsorption kinetics M.B. on Langmuir and Freundlich model.

Table 2: M.B. adsorption pseudomodel fit analysis.

Adsorbents	Pseudofirst-order model			Pseudosecond-order model		
	q_1 (mg/g)	K_1 (min^{-1})	R^2	q_2 (mg/g)	K_2 (min^{-1})	R^2
Biochar	120.65	0.254	0.982	118.56	0.0032	0.954
MgO/biochar	125.87	0.088	0.954	123.52	0.0025	0.895
Ag/MgO/biochar	98.54	0.045	0.991	86.54	0.0004	0.925

Table 3: Best fit analysis for Langmuir and Freundlich model adsorption kinetics.

Adsorbents	Langmuir model			Freundlich model			q_e (mg/g)
	q_1 (mg/g)	K_1 (min^{-1})	R^2	q_2 (mg/g)	K_2 (min^{-1})	R^2	
Biochar	126.45	25.4	0.952	105.78	0.115	0.936	132.62
MgO/biochar	132.57	13.26	0.924	118.65	0.123	0.974	145.69
Ag/MgO/biochar	102.32	5.32	0.961	65.65	0.975	0.962	122.58

Table 4: M.B. adsorption Langmuir model and Freundlich model.

Adsorbents	Langmuir model			Freundlich model			q_{exp} (mg/g)
	q_L (mg/g)	$K_{L(L/mg)}$	R^2	(mg/g)/(mg/L)^n	n	R^2	
Biochar	130.25	18.54	0.980	105.41	0.0625	0.954	132.65
MgO/biochar	148.25	2.542	0.965	132.65	0.0526	0.895	156.35
Ag/MgO/biochar	155.68	0.524	0.990	152.34	0.0449	0.925	165.32

nanocomposites. Conversely, insufficient loading may prime the combination of MgO nanoparticles on the exterior of the nanocomposites (Figure 8), limiting the surface area and closing the porosity to prevent M.B. adsorption.

3.4. Photocatalytic Degradation. Photocatalytic degradation of T.C. in Ag/MgO/biochar nanocomposites has been affected by different process parameters such as pH variations, T.C. concentration, Ag/MgO/biochar mixture ratio in percentage, temperature levels, and H_2O_2 conditions for removal of T.C. The pH was measured after photolysis of 100 ppm T.C. for 1 h, as it is considered to have a significant impact on the degradation as it affects the photocatalyst's surface possessions and capability to transfer electrons. The

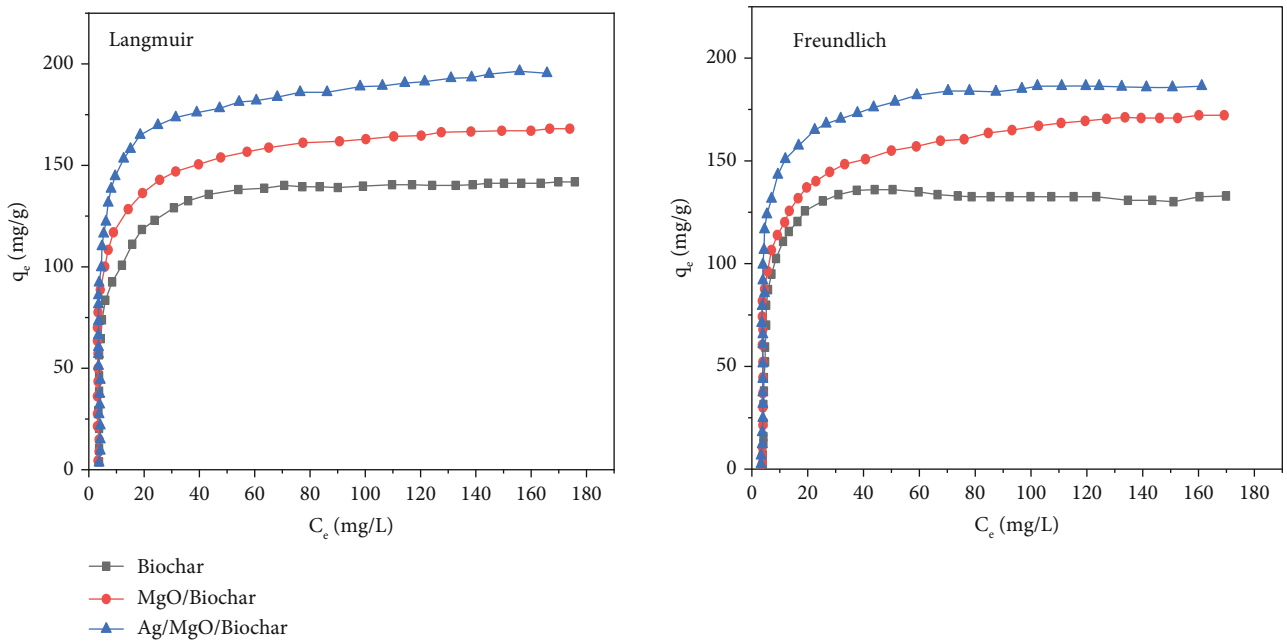

Figure 8: Adsorption isothermal.

T.C. removal efficiency for various pH levels of pH_2, pH_4, pH_6, and pH 8 is 28.13%, 32.15%, and 80.26%, respectively. At an acidic pH level (pH 8), it decreased to about 50.47%, which can be explained by the fact that H_2O_2 decomposes to O_2 rather than generating O.H. molecules, which are essential for the photosynthesis of T.C. It is important evident that Ag/MgO/biochar different proportions as a photocatalyst for degradation of T.C. for different pH levels accordingly shown in Figures 9(a) and 9(b).

Similarly, for all test conditions with initial T.C. concentration from 25 to 75 ppm, photocatalytic degradation efficiency was achieved to 80.24% for pH 6 at various times 30, 60, and 80 min for 25, 50, and 75 ppm, respectively. Figure 9(b) clearly shows the high efficiency of T.C.'s Ag/MgO/biochar removal under various concentrations. The objective of the present study was to investigate the effect of dosage variation of Ag/MgO@BC on the efficiency of T.C. removal by photocatalytic degradation of 50 ppm T.C. at pH 6 in 1 h (Figures 10(a) and 10(b)). The photocatalytic degradation efficiency increased from 47.68 to 62.88 and 80.24%, respectively, as the catalyst dosages increased from 0.005 to 0.0075 g and 0.01 g.

It can be concluded that the enhanced formation of hydroxyl free radicals causes faster photosynthetic degradation when the temperature is raised. Figure 11(a), depicting the effect of process temperature, demonstrates the efficiency of T.C. extraction at a heating rate of 10°C with a dose of 50 ppm in 1 h at pH 6. Whenever the temperature increased to 30°C, the efficiency increased and reached almost 80.2%. Also, at a significantly higher rate and an identical percentage of deterioration, the temperature reached 50°C. When the effect of temperature was studied in the absence of Ag/MgO@BC, the removal percentage was only about 14%, as shown in Figure 12, indicating that the minimum temperature had little effect on the T.C. decomposition rate. The remaining studies used moderate temperatures (25°C) to simulate actual conditions found in wastewater disposal operations.

During the T.C. photocatalytic degradation process, the H_2O_2 experiment was conducted for dissimilar absorptions 25, 50, 75, and 100 mM under pH 6 for 1 hour, as shown in Figures 11(a) and 11(b). The observed degradation rate was close to 52.25% at the lowest dose. When the amount of H_2O_2 was raised to 50, 75, and 100 mM, the degradation % suddenly increased to 54.24%, 66.24%, and 80.24%. The effect of H_2O_2 on the removal of T.C. is enhanced as it provides a photocatalytic degradation system with hydroxyls due to the widespread activity of hydroxyl families.

Furthermore, Ag/MgO/biochar recyclability and flexibility photocatalyst experimented for 1 hour under pH 6 for degradation of 50 ppm. The results show that the efficiency has reduced from 82.4% to 64.28% after a few usage cycles, indicating the reusability of Ag/MgO/biochar nanocomposites. It should be clarified that biochar accelerates the regeneration process of AgNPs and MgO N.P.s to achieve slow degradation efficiency for T.C. removal.

3.5. Future Scope and Recommendations. As a low-cost alternative to expensive activated charcoal, using biochar to remove pollutants from water is growing in significant importance. Future studies are needed to develop modified biochar, as the performance of this material varies depending on the type of raw materials used and the pyrolysis conditions. It may be possible to modify biochar properties to remove specific contaminants to increase their efficiency. Conservation of environmental research on bioenergy as a practical adsorbent for the removal of microbiological and metallic contaminants from water and gaseous particulate

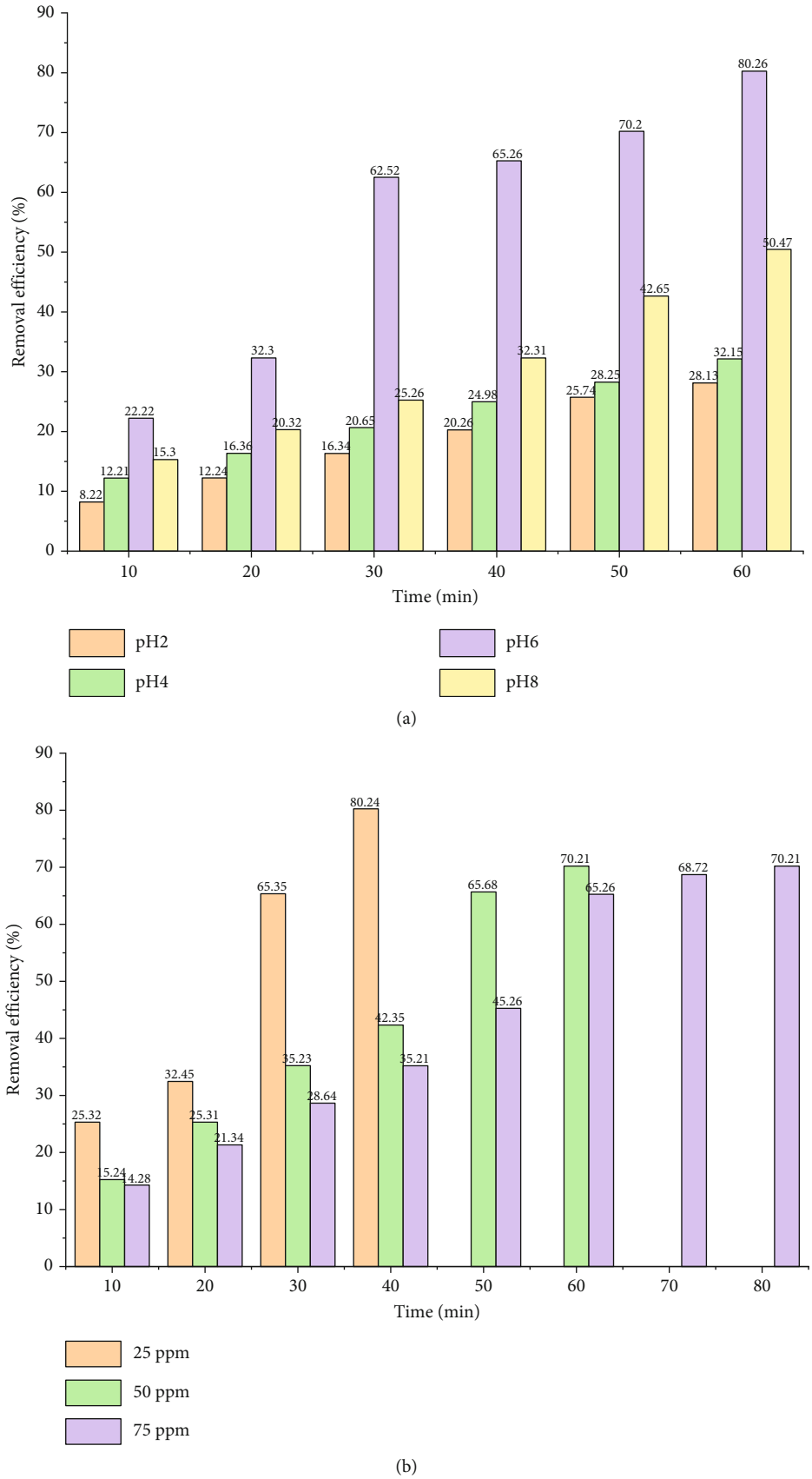

Figure 9: (a) Impact of pH on T.C. (b) Various ppm doses of Ag/MgO/biochar.

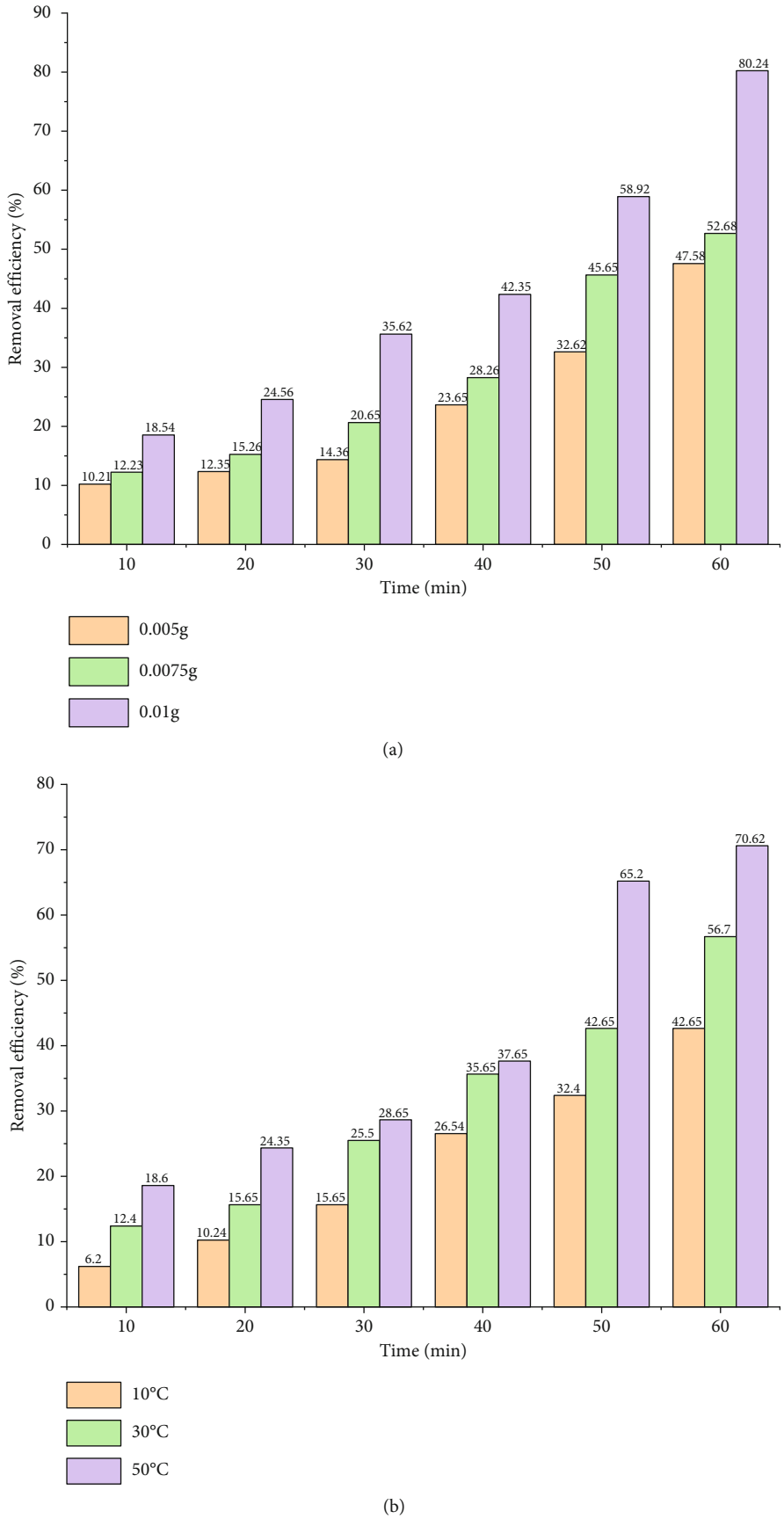

Figure 10: (a) Removal efficiency %. (b) Photocatalytic degradation temperature.

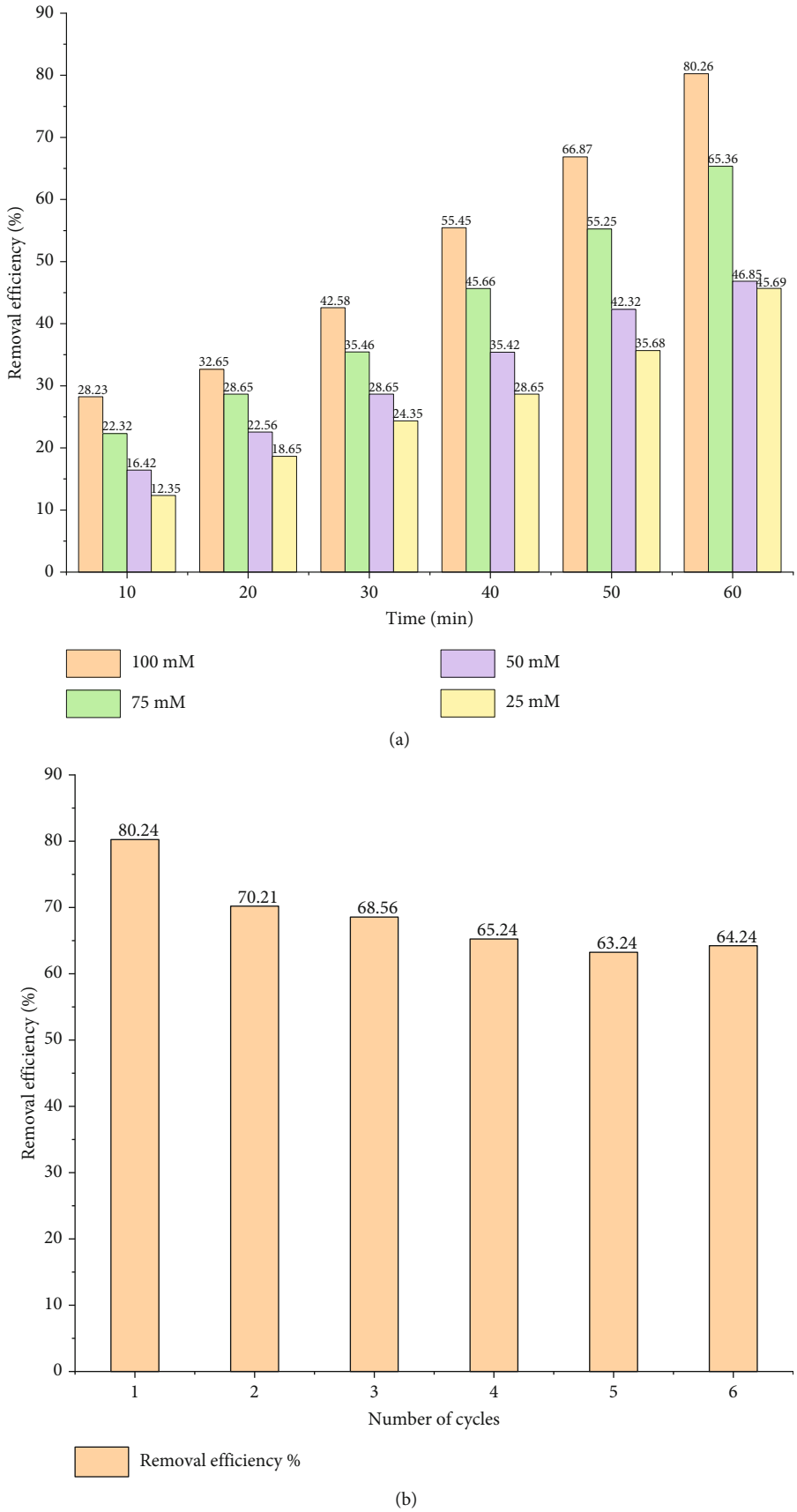

Figure 11: (a) Recyclability of Ag/MgO/biochar. (b) Photocatalytic degradation.

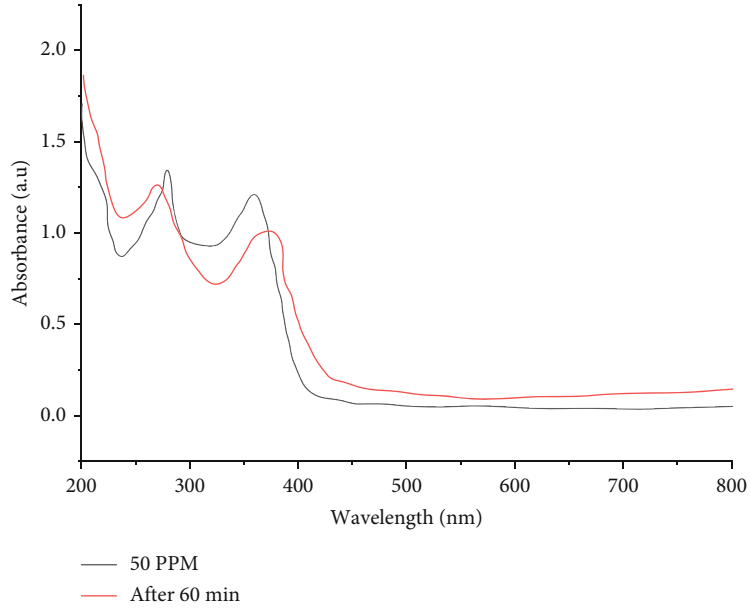

Figure 12: H_2O_2 removal efficiency.

pollution is extensive. Although the adsorption capacity of raw biochar is low, its physical and chemical properties are influenced by feed types and processing conditions.

4. Conclusions

The functional group of Ag/MgO/biochar nanocomposites was synthesized successfully by using solvent-free ball milling techniques for M.B. removal and photodegradation T.C. According to this investigation, the ball milling process provides greater flexibility and efficiency in a molecular and structural synthesis that can be used to remove natural and inorganic contaminants from the environment strategically. The successful synthesis of Ag/MgO/biochar nanostructures primarily removes M.B. by adsorption, which is controlled by an attractive electrostatic technique. Freundlich and Langmuir's features were used to match M.B. adsorption behaviour. Different models, with R^2 values above 0.91 and accurately characterizing isothermal, could not reveal any insight into the mechanisms underlying M.B. adsorption on MgO/biochar-nanostructured materials.

The results of this work show that ball-milled Ag/MgO/biochar nanocomposites are potential materials for removing dissolved organic substances from water. Adding MgO nanoparticles can efficiently generate the free radicals needed to break down highly concentrated M.B. in freshwater when exposed to light with the help of biochar. The Ag/MgO@BC exhibited significant performance under ideal process conditions, which included T.C. concentrations of 50 ppm, pH 6, Ag/MgO@BC dose of 0.01 g, the temperature of 25°C, and H2O2 concentration of 100 mM, Ag/ZnO@BC. The photocatalytic degradation of T.C. reaches 80.24%. Furthermore, the removal of M.B. from groundwater by nanocomposites depends on photosynthetic degradation.

Data Availability

The data used to support the findings of this study are included within the article.

Conflicts of Interest

The authors declare that there are no conflicts of interest regarding the publication of this paper.

References

[1] A. M. Omer, R. Dey, A. S. Eltaweil, E. M. Abd El-Monaem, and Z. M. Ziora, "Insights into recent advances of chitosan-based adsorbents for sustainable removal of heavy metals and anions," *Arabian Journal of Chemistry*, vol. 15, no. 2, article 103543, 2022.

[2] O. M. El-Borady, M. Fawzy, and M. Hosny, "Antioxidant, anticancer and enhanced photocatalytic potentials of gold nanoparticles biosynthesized by common reed leaf extract," *Applied Nanoscience*, vol. 1, pp. 1–12, 2021.

[3] M. Hosny, "Biogenic synthesis, characterization, antimicrobial, antioxidant, and catalytic applications of synthesized platinum nanoparticles (PtNPs) from Polygonum salicifolium leaves," *Journal of Environmental Chemical Engineering*, vol. 10, article 106806, 2022.

[4] E. M. Abd El-Monaem, "Sustainable adsorptive removal of antibiotic residues by chitosan composites: an insight into current developments and future recommendations," *Arabian Journal of Chemistry*, vol. 15, no. 5, article 103743, 2022.

[5] R. Li, J. J. Wang, B. Zhou et al., "Simultaneous capture removal of phosphate, ammonium and organic substances by MgO impregnated biochar and its potential use in swine wastewater treatment," *Journal of Cleaner Production*, vol. 147, pp. 96–107, 2017.

[6] R. Li, J. J. Wang, L. A. Gaston et al., "An overview of carbothermal synthesis of metal-biochar composites for the removal of

oxyanion contaminants from aqueous solution," *Carbon*, vol. 129, pp. 674–687, 2018.

[7] L. Natrayan, A. Merneedi, G. Bharathiraja, S. Kaliappan, D. Veeman, and P. Murugan, "Processing and characterization of carbon nanofibre composites for automotive applications," *Journal of Nanomaterials*, vol. 2021, Article ID 7323885, 7 pages, 2021.

[8] J. Shi, J. Wang, L. Liang et al., "Carbothermal synthesis of biochar-supported metallic silver for enhanced photocatalytic removal of methylene blue and antimicrobial efficacy," *Journal of Hazardous Materials*, vol. 401, article 123382, 2021.

[9] M. Kumar, X. Xiong, Z. Wan et al., "Ball milling as a mechanochemical technology for fabrication of novel biochar nanomaterials," *Bioresource Technology*, vol. 312, article 123613, 2020.

[10] D. Veeman, D. Dhamodharan, G. J. Surendhar, L. Natrayan, L. T. Jule, and R. Krishnaraj, "Systematic review on nine hallmarks of neurodegenerative disease," *Indian Journal of Biochemistry and Biophysics (IJBB)*, vol. 59, no. 3, pp. 249–257, 2022.

[11] Y. Zheng, Y. Wan, J. Chen, H. Chen, and B. Gao, "MgO modified biochar produced through ball milling: a dual-functional adsorbent for removal of different contaminants," *Chemosphere*, vol. 243, article 125344, 2020.

[12] C. A. Aggelopoulos, M. Dimitropoulos, A. Govatsi, L. Sygellou, C. D. Tsakiroglou, and S. N. Yannopoulos, "Influence of the surface-to-bulk defects ratio of ZnO and TiO_2 on their UV-mediated photocatalytic activity," *Applied Catalysis B: Environmental*, vol. 205, pp. 292–301, 2017.

[13] C. Ramesh, M. Vijayakumar, S. Alshahrani et al., "Performance enhancement of selective layer coated on solar absorber panel with reflector for water heater by response surface method: a case study," *Case Studies in Thermal Engineering*, vol. 36, article 102093, 2022.

[14] A. M. Omer, "Fabrication of easy separable and reusable MIL-125 (Ti)/MIL-53 (Fe) binary MOF/CNT/alginate composite microbeads for tetracycline removal from water bodies," *Scientific Reports*, vol. 11, pp. 1–14, 2021.

[15] J. Cao, L. Lai, B. Lai, G. Yao, X. Chen, and L. Song, "Degradation of tetracycline by peroxymonosulfate activated with zero-valent iron: performance, intermediates, toxicity and mechanism," *Chemical Engineering Journal*, vol. 364, pp. 45–56, 2019.

[16] Y. Chen, J. Q. Su, J. Zhang et al., "High-throughput profiling of antibiotic resistance gene dynamic in a drinking water river-reservoir system," *Water Research*, vol. 149, pp. 179–189, 2019.

[17] S. Palaniyappan, D. Veeman, S. Narain Kumar, G. J. Surendhar, and L. Natrayan, "Effect of printing characteristics for the incorporation of hexagonal-shaped lattice structure on the PLA polymeric material," *Journal of Thermoplastic Composite Materials*, vol. 1, no. article 08927057221089832, 2022.

[18] J. Dang, J. Guo, L. Wang et al., "Construction of Z-scheme Fe_3O_4/BiOCl/BiOI heterojunction with superior recyclability for improved photocatalytic activity towards tetracycline degradation," *Journal of Alloys and Compounds*, vol. 893, article 162251, 2022.

[19] Y. Luo, X. Wei, B. Gao et al., "Synergistic adsorption-photocatalysis processes of graphitic carbon nitrate (gC_3N_4) for contaminant removal: kinetics, models, and mechanisms," *Chemical Engineering Journal*, vol. 375, article 122019, 2019.

[20] S. L. James, C. J. Adams, C. Bolm et al., "Mechanochemistry: opportunities for new and cleaner synthesis," *Chemical Society Reviews*, vol. 41, no. 1, pp. 413–447, 2012.

[21] R. Venkatesh, C. Ramesh Kannan, S. Manivannan et al., "Synthesis and experimental investigations of tribological and corrosion performance of AZ61 magnesium alloy hybrid composites," *Journal of Nanomaterials*, vol. 2022, Article ID 6012518, 12 pages, 2022.

[22] M. M. Matheswaran, T. V. Arjunan, S. Muthusamy et al., "A case study on thermo-hydraulic performance of jet plate solar air heater using response surface methodology," *Case Studies in Thermal Engineering*, vol. 34, article 101983, 2022.

[23] C. Zhu, M. Takata, Y. Aoki, and H. Habazaki, "Nitrogen-doped porous carbon as-mediated by a facile solution combustion synthesis for supercapacitor and oxygen reduction electrocatalyst," *Chemical Engineering Journal*, vol. 350, pp. 278–289, 2018.